Supporting Material

Surfing along filopodia – a particle transport revealed by molecular scale fluctuation analyses

Felix Kohler[1,2] and Alexander Rohrbach[1,2]

[1] *Laboratory for Bio- and Nano-Photonics, Department of Microsystems Engineering , University of Freiburg, Germany*

[2] *Centre for Biological Signalling Studies (bioss), University of Freiburg, Germany*

S1 - Release of molecular bond

In the example examined here, the start of the transport is triggered by an abrupt displacement which probably corresponds to the release of a molecular binding.

			unit	x	y	z		
direct readouts	bead position before release	$\mathbf{r}'$	nm	150	107	-12		
	total stiffness before release	κ'	pN/µm	1170	530	500	mean	733
	total friction before release	γ'	pN ms/µm	1320	500	534		
	bead position after release	$\mathbf{r}''$	nm	269	171	184		
	total stiffness after release	κ''	pN/µm	380	220	250	mean	283
	total friction after release	γ'	pN ms/µm	104	45	35	mean	61
	trap position	$\mathbf{r}_{trap}$	nm	86	107	23		
	trap stiffness	κ_{opt}	pN/µm	51	53	10	mean	38
	relaxation time	τ_{off}	µs	186	175	303	mean	221
results	displacement of bead	$\mathbf{r}'-\mathbf{r}''$	nm	119	64	196	abs	238
	position of bond A*	$\mathbf{r}_A$	nm	93	62	-208		
	position of bond B*	$\mathbf{r}_B$	nm	297	191	191		
	distance between bonds*	$\mathbf{r}_A-\mathbf{r}_B$	nm	204	129	399	abs	466
	stiffness of bond A	κ_A	pN/µm	790	310	250	mean	450
	stiffness of bond B	κ_B	pN/µm	329	167	240	mean	245
	force of bond A before release	$\mathbf{F}'_A$	pN	-45	-14	-49	abs	68
	energy stored in bond A before release	G'_A	kT	304	75	1126	sum	1505
	force of bond B before release	$\mathbf{F}'_B$	pN	48	14	49	abs	70
	energy stored in bond B before release	G'_B	kT	838	139	1157	sum	2134
	force of bond B after release	$\mathbf{F}''_B$	pN	9	3	1	abs	10
	autocorrelation time	γ''/κ''	µs	274	203	140	mean	206

Table S1 Release of a bond at $t = t_{rest}$. Parameters read out from the trace and the fluctuations before and after $t=t_{rest}$. Resulting mean bead position using the mean position over 50ms, bead displacement, stiffnesses of bond A and B, appearing forces and relaxation times according to the model presented in the main text.

By means of the methods described in the main text, several parameters can be obtained directly from the beads' displacement and the analysis of the beads' fluctuations. These parameters are listed in Table S1 under "direct readouts". According to the mechanical model presented in the main text and illustrated in Fig. 4 values for the position, stiffness of the involved bonds as well as about the forces and energies stored in the bonds are listed in

addition. All values are stated in all spatial dimensions, where the x coordinate corresponds to the direction of the filopodial extension. When applicable, mean values or alternatively absolute (abs) or sum values are listed.

S2 - Actin flow in adherent filopodia

In an additional experiment, we used GFP life act actin labeled J774 cells, which we observed by another microscope in our lab equipped with total internal reflection fluorescence (TIRF). As shown in figure 5A, TIRF allows to identify single adherent filopodia with high contrast due to suppressed background fluorescence. The actin dynamics were recorded at a frame rate of 3.5 Hz and show a retrograde flow, which was further analyzed as shown by the exemplary kymograph in Fig. S1 B. The red dashed line indicates the velocity of the edge of a larger fluorescent speckle, which was determined to be v_{act} = 60nm/s.

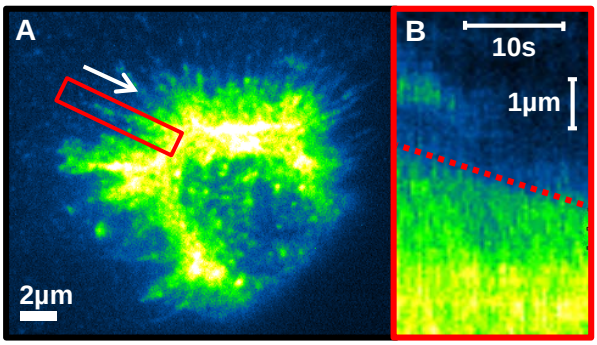

FIGURE S1 Retrograde actin flow inside adherent filopodia. *(A) TIRF image of GFP actin labeled cell. B) Kymograph along filopodium (marked region in A). The dashed line indicates the retraction of fluorescent front moving at a velocity of* v_{act} *= 60nm/s.*

S3 – Experimental setup

The setup is based on an inverted microscope (Axio Observer from Zeiss, Germany) which is placed together with the 1064nm laser (Smart Laser Systems, Germany) and the optical elements necessary for laser stabilization, modification and steering on a passively air damped table (Newport, United States). The central elements of the setup are the trapping objective (TO) (C-Apochromat 63x/1.20W Corr M27, Zeiss, Germany) and the detection objective (DO) (W Plan-Apochromat 63x/1.0, Zeiss, Germany), which are aligned confocally (Fig. S2). The focal plane, where the sample is placed and the actual experiment takes place, is located between these objectives. To avoid drifts and damages due to misuse, the z-drive has been fixed at the position of confocal arrangement. As shown in Fig. S2, the cover slip which carries the cells is mounted on a removable insert of anodized aluminum. This insert is capable to capture approximately 1*ml* of liquid. The temperature of this liquid can be controlled by a ring shaped heating element (TC-CSC, bioscience tools, United States) which retains the insert and by a heatable cab on the detection objective. Both heating elements have integrated temperature sensors and are controlled by a PID controller

(TC-2-100 from bioscience tools, United States). The heating element which carries the removable insert is connected to a 3 axis piezo stage (Nano-LPS200, Mad City Labs, United States) with a sandwich of fiber reinforced polymer plates which have a low thermal conductivity. This design assures a constant temperature of the sample, usually chosen to be 37°C for the cell experiments, without a relevant heating of the sensitive surrounding parts and without causing drifts. The heating system is switched on about 1*h* prior to the experiment to allow the system to equilibrate.

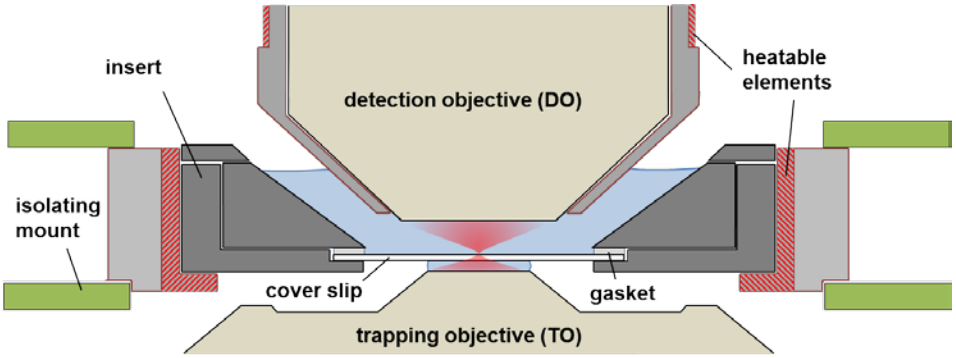

FIGURE S2 The central part of the setup including the sample mount is illustrated by a cut through a vertical plane, where radial symmetry applies. The round insert made of anodized aluminum is shown in dark gray, the water or cell culture medium is shown in blue, the heating unit and the heatable cab are shown in light gray, and the fiber-reinforced polymer plates are shown in green.

S4 – Transport of beads along filopodia

The results presented in Figures 1 to 8 are based on one exemplarily experiment. In this experiment the stiffness during the rest time is significantly higher than at the beginning of the transport, which constitutes a special but informative case. In Fig. S3 and Fig. S4 two transport events are shown, where the start of the transport is not accompanied by a decrease but rather by a slight increase of the stiffness.

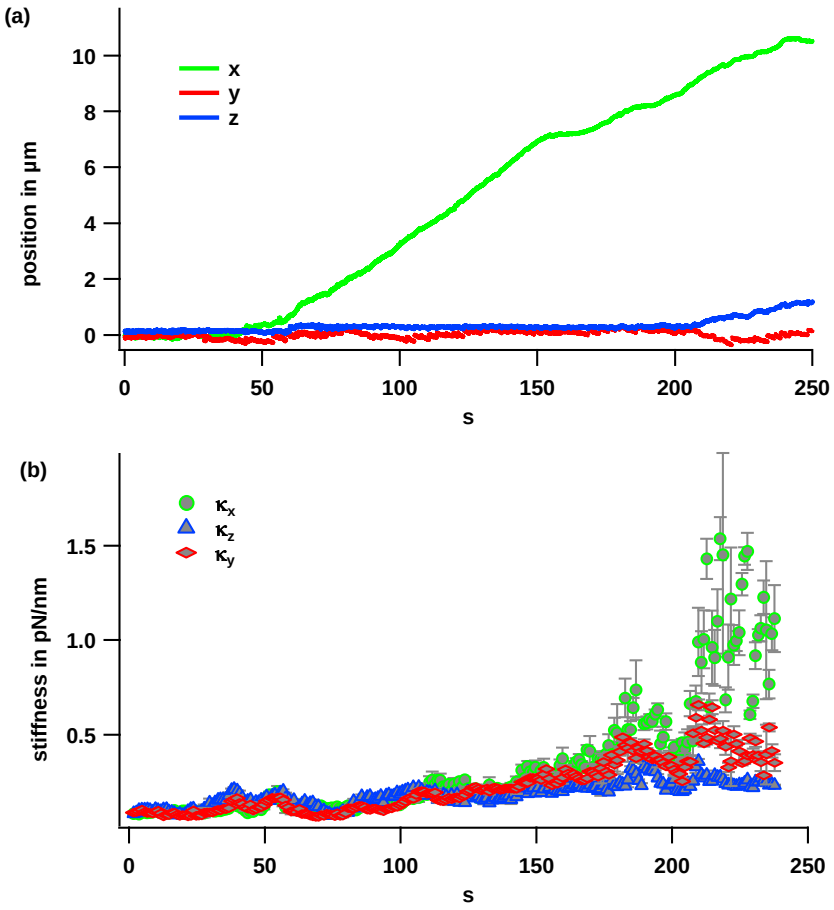

Figure S3 Bead position (a) and stiffness parameter (b) as a function of time. The data shown corresponds to data 6 in Table 1.

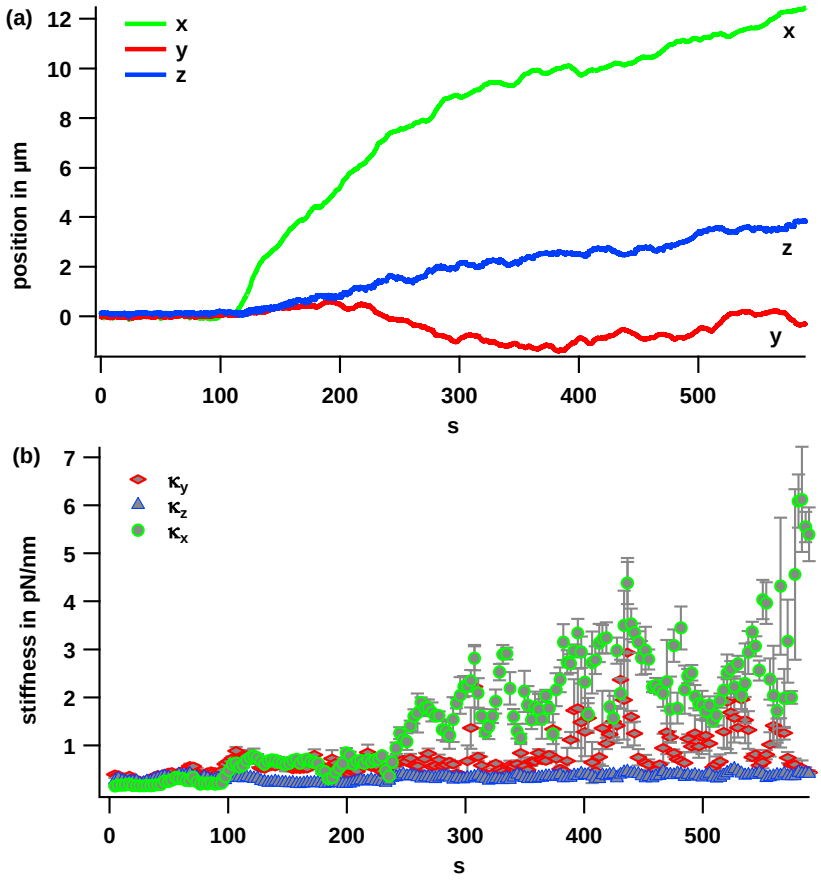

Figure S4 Bead position (a) and stiffness parameter (b) as a function of time. The data shown corresponds to data 7 in Table 1.

S5 – Stiffness changes during rest time

In about half of the cases, it was possible to move the bead along a filopodium before it got stuck at a certain point. The measured stiffness values before and after the point in time when the bead got stuck are shown in Table S2. The stiffness increases by more than a factor of 6 in lateral directions and by 65% in direction perpendicular to the cell membrane.

stiffness in pN/µm	**x**	**y**	**z**	**mean**
rest time movable	19	21	32	24
rest time fixed	137	128	53	106
transport	229	153	64	149

Table S2 Stiffness variations during experiment. Stiffness values in the 3 spatial dimensions are shown for an experiment, in which the bead is first moved along the filopodia be means of the optical trap (movable) until the bead got stuck and could not be moved any further (fixed). The values are additionally compared to the stiffness values during bead transport.

The increase in stiffness is likely due to an additional binding, e.g., by an adhesion patch which hinders the fluctuations of the bead.

S6 - Backbone as mechanical coupler between myosin work and polymerization

Assuming that myosin motors are responsible for the transport of the filopodial backbone, an important question is how the polymerization rate in the tip f_{poly} and the mean myosin step rate f_{step} in the cell cortex affect each other. The only mechanical connection between the cortical myosin and the filopodium tip is the actin backbone as indicated in Fig. 1 A. Assuming a permanent linkage of the bead to the actin backbone, the varying velocity of the bead $v_b(\mathrm{t})$ (see Fig. 2 A or 6 E) reflects the retrograde movement of the actin backbone. The actin backbone polymerizes at the tip with a velocity v_{poly}. A polymerization velocity v_{poly} exceeding the velocity $v_b(\mathrm{t})$ of the backbone over a longer period of time would lead to a growth of the adherent filopodium, which has not been observed in our experiments. A polymerization velocity falling below v_b for a certain period of time would lead to large gaps between the end of the backbone and the membrane at the tip. Such large gaps would lead to a total disconnection of the tip complex from the actin backbone, which seems to be an unlikely situation (see also (1)). This strengthens the idea of the mechanical coupling between the transport machinery and the polymerization at the filopodial tip which leads to $v_{poly} \approx v_b$. Assuming equal velocities ($v_{poly} \approx v_b$) for an adherent filopodium, any variation of the transport speed v_b, controlled by the cortical myosin, must affect (regulate) the mean polymerization speed $v_{poly} \sim f_{poly}$ in the filopodium tip, provided the backbone is disconnected only very shortly from the tip (2, 3) and the gap length hardly changes. Depending on the concentration of actin monomers in the tip, the polymerization rate f_{poly} is limited differently by diffusion and reaction. To a smaller extent, the polymerization in the tip towards the membrane exerts also a force on the myosin motors at the backbone shaft, thereby affecting their stepping rate. Yet, further research in this direction is required to clearly prove this mechanical coupling.

On longer timescales, other affecting proteins inside the filopodium such as Cdc42, ENA/VASP, FMNL2 regulate the actin polymerization in addition. However this diffusion-based regulation process takes significantly longer than a direct mechanical connection via the actin backbone. However, any counteracting forces F as opposed, e.g., by the optical trap, by other external bonds or by intracellular clutch mechanisms (4), will affect the transport speed $v_b(\mathrm{F})$ or, assuming a stepwise movement, the mean step rate $f_{step}(F)$ of the backbone resulting in a mean force dependent polymerization rate $f_{poly}(F) = 2v_b(F)/a = 2f_{step}(F) \cdot \Delta x_{myo}/a$ per filament at the tip. Here a = 5.4 nm is the length of the actin monomers and Δx_{myo} is the mean step size of myosin, which is assumed to be responsible for the transport. These dependencies have been investigated for dorsal filopodia (1), although here a direct mechanical coupling through the backbone was not shown either. The bead velocity $\overline{v}_b$ = 60 nm/s (see Table 1) coincides well with the measured retrograde velocity of a GFP-actin speckle inside an adherent filopodium we observed with TIRF (see S2).

Supporting References

1. Bornschlögl, T., S. Romero, C.L. Vestergaard, J.-F. Joanny, G. Tran Van Nhieu, et al. 2013. Filopodial retraction force is generated by cortical actin dynamics and controlled by reversible tethering at the tip. Proc. Natl. Acad. Sci. 110: 18928–18933.

2. Medalia, O., M. Beck, M. Ecke, I. Weber, R. Neujahr, et al. 2007. Organization of actin networks in intact filopodia. Curr. Biol. 17: 79–84.

3. Yang, C., M. Hoelzle, A. Disanza, G. Scita, and T. Svitkina. 2009. Coordination of membrane and actin cytoskeleton dynamics during filopodia protrusion. PLoS One. 4: e5678.

4. Chan, C.E., and D.J. Odde. 2008. Traction dynamics of filopodia on compliant substrates. Science. 322: 1687–91.